

# Anharmonicity in Thermal Insulators – An Analysis from First Principles

Florian Knoop,<sup>1,2</sup> Thomas A. R. Purcell,<sup>1</sup> Matthias Scheffler,<sup>1</sup> and Christian Carbogno<sup>1</sup>

<sup>1</sup>*The NOMAD Laboratory at the FHI of the Max-Planck-Gesellschaft and IRIS-Adlershof of the Humboldt-Universität zu Berlin, Faradayweg 4-6, 14195 Berlin, Germany*

<sup>2</sup>*Theoretical Physics Division, Department of Physics, Chemistry and Biology (IFM), Linköping University, SE-581 83 Linköping, Sweden*

(Dated: April 27, 2023)

The anharmonicity of atomic motion limits the thermal conductivity in crystalline solids. However, a microscopic understanding of the mechanisms active in strong thermal insulators is lacking. In this letter, we classify 465 experimentally known materials with respect to their anharmonicity and perform fully anharmonic *ab initio* Green-Kubo calculations for 58 of them, finding 28 thermal insulators with  $\kappa < 10$  W/mK including 6 with ultralow  $\kappa \lesssim 1$  W/mK. Our analysis reveals that the underlying strong anharmonic dynamics is driven by the exploration of meta-stable intrinsic defect geometries. This is at variance with the frequently applied perturbative approach, in which the dynamics is assumed to evolve around a single stable geometry.

Efficient energy conversion is one of the key challenges for the 21<sup>st</sup> century. In this context, the thermal conductivity  $\kappa$  is an important material property that can strongly influence device performance and efficiency. This is the case, for example, in combustion engines, where thermal barrier coatings are used to increase operating temperatures [1, 2], or in thermoelectric materials for waste-heat recovery [3]. In both cases, strong thermal insulators are required and the best available materials intrinsically have a low  $\kappa < 10$  W/mK. Additional defect and grain boundary engineering can reduce  $\kappa$  even further [4, 5]. Since heat transport is limited by effects beyond the harmonic phonon picture [6], elucidating the microscopic anharmonic mechanisms leading to a low intrinsic thermal conductivity is a prerequisite for searching the next generation of thermal insulators. However, our current knowledge about thermal insulators is rather limited. Experimental measurements are hindered by the challenge of growing macroscopic, well-characterized samples [7]. In turn, Springer Materials lists only a little over one thousand measurements for all inorganic solids, and just a few hundred semiconductors and insulators are characterized well at ambient conditions [8, 9].

One way to expand on this knowledge is via computational materials discovery based on (high-throughput) screening of chemical space that is accelerated by artificial-intelligence techniques [10–12]. To this end, reliable simulations of lattice thermal conductivities in the sub-10 W/mK regime are necessary. Typically, Peierls-Boltzmann [13, 14] or Wigner-type [15, 16] approaches based on a (renormalized [17]) phonon-picture are employed for this purpose. However, these methods are only applicable as long as the phonon quasi-particle picture is valid, i. e., when the phonon lifetime exceeds the vibration period, as formulated within the Ioffe-Regel limit [16, 18]. In this letter, we demonstrate that the presence of metastable defect geometries is associated with strong anharmonic effects, which break the Ioffe-

Regel limit and result in the exploration of different energy minima. This breakdown of the phonon picture leads to unexpectedly low thermal conductivities.

To this end, we employ the *ab initio* Green-Kubo (aiGK) method which is not affected by the aforementioned limitations since the atomic motion is evaluated via *ab initio* molecular dynamics (aiMD) simulations [19, 20]. Here, we benchmark and validate the approach for 24 crystalline materials for which reliable experimental measurements are available, showing that the necessary accuracy to predict materials in the sub-10 W/mK regime can be reached, even when the phonon picture is no longer valid. We subsequently devise a hierarchical screening strategy to search for strongly anharmonic thermal insulators in a chemically and structurally diverse space of materials that covers 465 experimentally known compounds that are stable at ambient conditions, but without experimentally known  $\kappa$ . By that, we identify 28 materials with  $\kappa < 10$  W/mK and we discuss the role of structural displacements to meta-stable geometries for the underlying strongly anharmonic dynamics.

The aiGK approach evaluates the Green-Kubo (GK) equation [21, 22]

$$\kappa(T) = \frac{V}{3k_{\text{B}}T^2} \lim_{t_0 \rightarrow \infty} \int_0^{t_0} \langle \mathbf{J}(t) \cdot \mathbf{J}(0) \rangle_T dt, \quad (1)$$

with the heat flux  $\mathbf{J}(t)$ , volume  $V$ , temperature  $T$ , and Boltzmann constant  $k_{\text{B}}$ . Here,  $\langle \bullet \rangle_T$  denotes an ensemble average. In this work, the heat flux  $\mathbf{J}(t)$  is computed from first principles along aiMD trajectories using the formalism defined in Ref. [20]. We use the *FHI-aims* code [23, 24] and the PBEsol [25] exchange-correlation functional. By neglecting convective contributions to  $\mathbf{J}(t)$ , which are usually negligible in solids [26], physically well-founded strategies to overcome finite-size and -time effects can be established. This includes noise-filtering of the integrand in Eq. (1), i. e., the heat flux autocorrelation function (HFACF), and accounting for long-wavelength excitations missing in the simulation cell

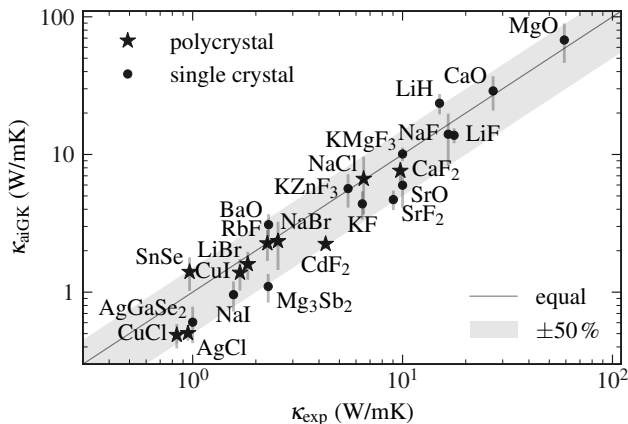


FIG. 1. Correlation between measured (● single-crystals, ★ polycrystals) and computed (aiGK) thermal conductivities at room temperature on a log-log scale. The gray area indicates 50% deviation in terms of  $\kappa$  from experiment and the error bars denote the standard error between trajectories. Where multiple experimental references were available, the average was taken.

via reciprocal-space interpolation [20] as discussed in detail in a separate work [27] and implemented in *FHI-vibes* [28]. Computational parameters were chosen to obtain reliable values of  $\kappa$  at room temperature: All aiMD simulations are performed in extended supercells (160–256 atoms) with trajectory lengths of up to 60 ps. Error bars are estimated by ensemble averaging over at least three independent trajectories. Lattice expansion is accounted for by minimizing the thermal pressure at 300 K [29]. Further details are given in the supplemental material (SM) [30].

To benchmark the aiGK approach, we investigate 24 dielectric compounds, for which experimental values of the bulk thermal conductivity  $\kappa$  at room temperature are reported in the literature [30]. The reference data covers two orders of magnitude in  $\kappa$ , but also carries an uncertainty which is rooted in differences in sample quality and experimental techniques [9]. For instance, available data for tin selenide (SnSe) varies by up to 50% [7]. As shown in Fig. 1, the aiGK calculations provide a satisfactory agreement with experiment over the whole range of  $\kappa$ : For mildly anharmonic conductors with  $\kappa > 20$  W/mK, the quality of the predictions [mean absolute percentage error (MAPE) of 22%] is on par with results from advanced perturbative methods [31, 32]. Good accuracy is retained also for strongly insulating materials with  $\kappa < 20$  W/mK, which show a comparable MAPE of 28% and a resulting mean absolute error (MAE) of just 1 W/mK. Accounting for strongly anharmonic effects is decisive to reach this accuracy in the sub-10 W/mK regime, as exemplified by the fact that the aiGK method correctly predicts  $\kappa$  to be 1.4 W/mK for copper iodide (CuI), just 16% smaller than in experiment. In con-

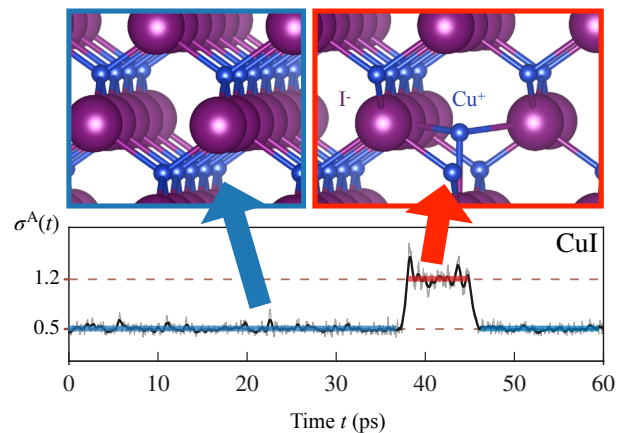


FIG. 2. Anharmonicity measure  $\sigma^A(t)$  for CuI evaluated at each time step during one aiMD trajectory. The upper row shows averaged positions in  $(10\bar{1})$  direction for time-periods with  $\sigma^A(t) \approx 0.5$  (blue), and increased  $\sigma^A(t) \approx 1.2$  (red), in which one Cu cation moves to an interstitial site along  $(\bar{1}11)$ .

trast, different phonon-based approaches yield values between 5.8 and 6.8 W/mK, overestimating experiment by  $\gtrsim 350\%$ , cf. SM Sec. IV. Even more importantly, the accurate lifetimes obtained from fully anharmonic aiMD reveal a breakdown of the phonon picture in this compound, cf. SM Sec. VI.

For CuI, an analysis of the aiMD dynamics confirms that strong anharmonic effects are at play: Figure 2 shows the time evolution of the anharmonicity measure  $\sigma^A(t)$  introduced in Ref. [33], which quantifies the differences between the actual and the harmonic potential-energy surface (PES) and hence would vanish in perfectly harmonic materials [30, 33]. The sudden increase of  $\sigma^A(t)$  from its value of 0.5 to 1.2 signals that the harmonic approximation becomes qualitatively incapable to describe the dynamics: In this several picoseconds long period, a meta-stable Frenkel defect is formed [34]. As shown in Fig. 2, one Cu cation moves to an interstitial site along the  $(\bar{1}11)$  direction and vibrates around this meta-stable defect geometry, before it jumps back to the zincblende equilibrium configuration associated with  $\sigma^A(t) \approx 0.5$ . This temporary defect formation may be viewed as a local precursor of the superionic  $\beta$ -phase of CuI, which is known to exhibit a considerable defect concentration  $> 10\%$ , but only becomes stable at significantly higher temperatures ( $> 643$  K) [35].

In the next step, we employ the aiGK method to screen for thermal insulators via a hierarchical workflow: We study 465 experimentally known binary and ternary materials for which  $\kappa$  at room temperature has not been measured. This set of materials covers seven space groups (62, 122, 166, 186, 216, 221, 225), including not only simple rock salt materials with two atoms per unit cell, but also more complex compounds, e. g., or-

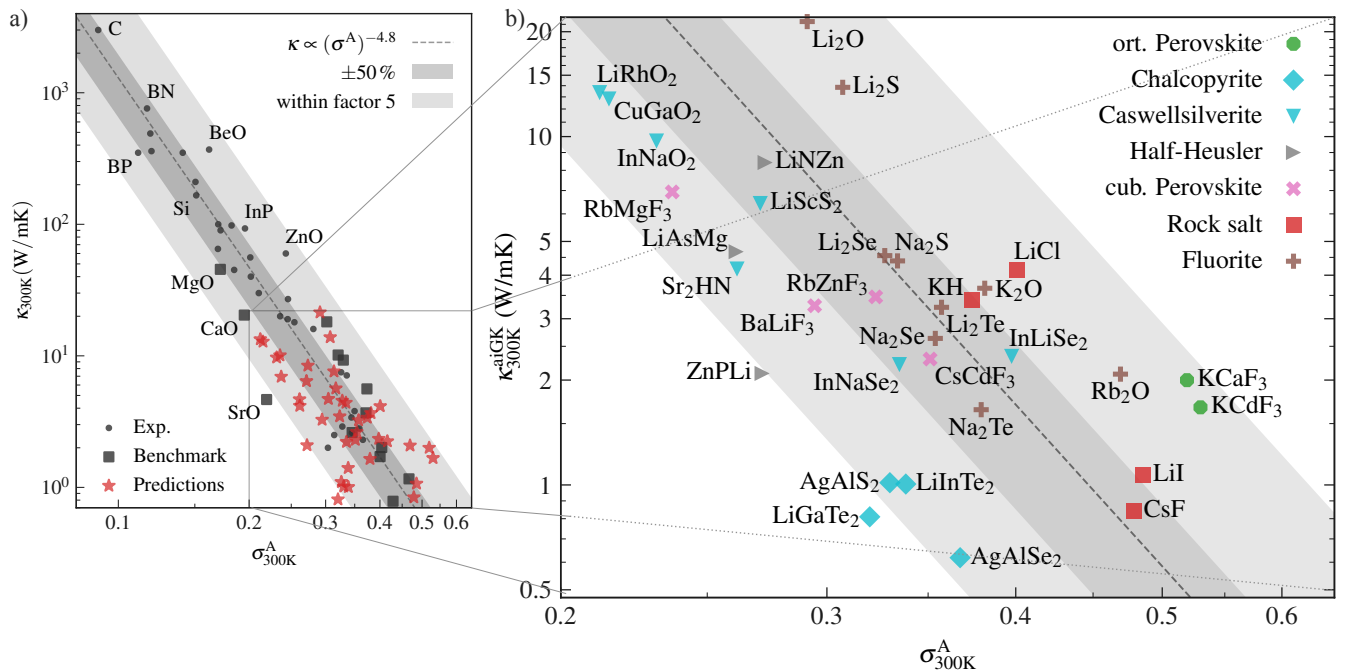


FIG. 3. Thermal conductivity  $\kappa$  vs. anharmonicity at 300 K,  $\sigma_{300\text{K}}^A$  (tabulated data given in the SM [30]). The dashed trend line and grey areas are shown to guide the eye. a) The qualitative scaling of  $\kappa$  with  $\sigma_{300\text{K}}^A$  suggested in Ref. [33] and used to disregard good thermal conductors during screening is showcased using experimental measurements (black  $\bullet$ ) as well as our aiGK calculations [black  $\blacksquare$ : benchmarks from Fig. 1; red  $\star$ : predictions from subplot (b)]. b) Thermal conductivity aiGK predictions for materials with  $\sigma_{300\text{K}}^A > 0.2$ . The symbol and color code indicate the lattice type.

thorombic perovskites with 20 atoms in the unit cell. Note that only materials with elements lighter than Lanthanum are considered to avoid potential artifacts in the dynamics associated to the treatment of spin-orbit coupling. First, we compute the band gap and the anharmonicity measure at 300 K,  $\sigma_{300\text{K}}^A$ , for all 465 compounds. The results cover the range  $\sigma_{300\text{K}}^A = 0.1 - 0.7$ , cf. SM. Over 50% of the materials feature an anharmonicity of  $\sigma_{300\text{K}}^A \approx 0.23$  or less, in line with Ref. [33]. Second, we exclude materials with DFT-PBEsol band gaps below 0.2 eV to ensure that electronic contributions to heat transport are negligible and we discard more harmonic materials with  $\sigma_{300\text{K}}^A < 0.2$  to avoid unnecessary and expensive calculations, since those materials can be expected to be good thermal conductors [33] that can be treated with perturbative approaches. The first aspect is substantiated by Fig. 3a, which shows that the materials with  $\sigma_{300\text{K}}^A < 0.2$  feature  $\kappa$  values (much) larger than 10 W/mK. From the remaining  $\sigma_{300\text{K}}^A > 0.2$  pool, we generate a diverse test set of materials that uniformly cover the range  $\sigma_{300\text{K}}^A = 0.2 - 0.6$ . Materials with a particularly slow phonon dynamics were excluded to ensure that simulation time convergence can be reached within reasonable trajectory lengths  $\leq 60$  ps, as detailed in the SM [30]. Finally, we obtain thermal conductivities for 34 materials for which  $\kappa$  has *not* been measured yet, see Fig. 3b.

Although the  $\sigma^A$ -criterion is only qualitatively valid for the identification of thermal insulators, no good thermal conductors are found within this set. On the contrary, we find 28 new materials with a thermal conductivity of  $\kappa_{\text{aiGK}} < 10$  W/mK, 6 of which with an ultralow conductivity  $\lesssim 1$  W/mK. These compounds comprise simple binary, cubic materials such as the rock salts CsF and LiI or the fluorite  $\text{Na}_2\text{Te}$ , but also more complex structures such as the  $\text{KCdF}_3$  and  $\text{KCaF}_3$  perovskites. Furthermore, we find four chalcopyrites ( $\text{AgAlSe}_2$ ,  $\text{AgAlS}_2$ ,  $\text{LiGaTe}_2$ ,  $\text{LiInTe}_2$ ), a material class that has recently gained interest for thermoelectric applications [36–38]. In the strongly insulating regime shown in Fig. 3b, the simple power-law correlation between  $\kappa$  and  $\sigma_{300\text{K}}^A$  observed in Fig. 3a is no longer valid due to the increased variety and complexity of the compounds. This can be explained by comparing two materials ( $\text{LiGaTe}_2$ ,  $\text{KCaF}_3$ ); more details are given in the SM [30]: The strongly insulating character of the chalcopyrite  $\text{LiGaTe}_2$  ( $\kappa_{\text{aiGK}} = 0.8$  W/mK) can already be rationalized in a harmonic picture, since most phonon branches of this compound, including the acoustic ones, exhibit only an extremely weak dispersion, cf. Suppl. Fig. 1. Accordingly, only few modes with  $\omega < 4$  THz can contribute to thermal transport, and even these feature very low group velocity  $\lesssim 1.5$  km/s, cf. Suppl. Fig. 2. Since this is a common property in chalcopyrites, Plata *et al.* were able to correctly pre-

dict thermal insulators in this material class [37], even if the employed perturbative approach might overestimate  $\kappa$  due to the low-order description of anharmonicity. In comparison,  $\text{KCaF}_3$  features much more dispersive phonon frequencies: The majority of modes across the whole frequency range contributes to heat transport with considerably larger group velocities that reach 5 km/s, suggesting a moderately good thermal conduction. In this case, the strongly insulating character of  $\text{KCaF}_3$  ( $\kappa_{\text{aiGK}} = 2 \text{ W/mK}$ ) can only be explained by its strong anharmonicity ( $\sigma_{300\text{K}}^A = 0.5$ ), which results in extremely low phonon lifetimes  $\lesssim 1 \text{ ps}$ . As shown in Fig. 4, this is reflected in the real-space dynamics that displays temporary rearrangements towards different, meta-stable configurations. These involve an increase of  $\sigma^A(t)$ , as discussed above for CuI in Fig. 2. Unlike CuI however, in which these rearrangements correspond to the formation of intrinsic point defects, we observe more extended distortions in  $\text{KCaF}_3$  that span multiple primitive unit cells, cf. Fig. 4. As discussed in the SM, these configurations are associated to reorientations of the  $\text{CaF}_3$  octahedra into different, nearly-degenerate octahedral tilting patterns. These meta-stable configurations are a common feature of perovskite materials and their dynamics often leads to the stabilization of higher-temperature phases [39, 40]. For  $\text{KCaF}_3$ , the described dynamics is a precursor of the cubic phase, which becomes stable at temperatures  $> 550 \text{ K}$  [41].

Note that these temporary atomic rearrangements into meta-stable geometries are not observed in all trajectories. Nonetheless, their microscopic origin, i.e., a strongly-anharmonic PES featuring multiple minima, influences the whole dynamics. Even when these minima are not explicitly explored, harmonic and anharmonic contributions are at least of equal importance, as signaled by the high  $\sigma^A$  value  $\geq 0.5$ , and the fact that the fully anharmonic lifetimes, which violate the Ioffe-Regel limit in both compounds, demonstrate a breakdown of the phonon picture, as shown in Suppl. Fig. 3 and Sec. VI in the SM. These observations are direct evidence that the existence of barely accessible meta-stable states is sufficient to increase the anharmonicity in CuI and  $\text{KCaF}_3$  beyond the level at which it can be treated as a perturbation. We also note that these localized effects are different from other local, anharmonic scattering mechanisms such as “rattlers” that do not involve temporal lattice distortions [42].

In summary, we presented a comprehensive set of aiGK calculations to search for thermal insulators. By hierarchically screening over 465 experimentally known materials, we identified 28 new materials with  $\kappa < 10 \text{ W/mK}$  including 6 compounds with ultralow  $\kappa \lesssim 1 \text{ W/mK}$ . Our analysis reveals that the dynamics in many thermal insulators is not limited to displacements around a *single*, stable equilibrium geometry, as assumed in perturbative approaches like the Boltzmann transport equation (BTE).

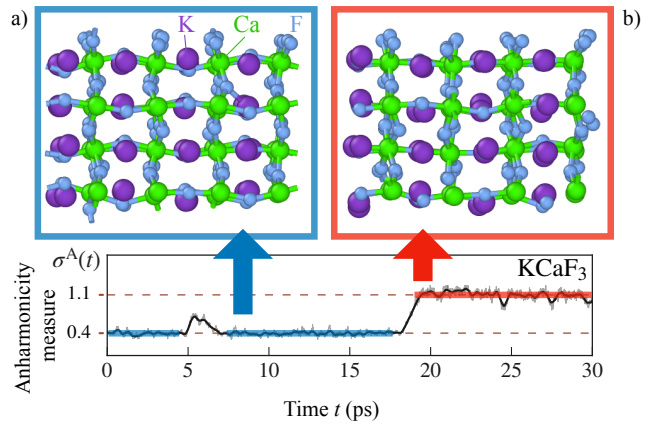


FIG. 4. Anharmonicity measure  $\sigma^A(t)$  for  $\text{KCaF}_3$  evaluated at each time step during one aiMD trajectory. The upper row shows time-averaged positions in (100) direction for the periods with a)  $\sigma^A(t) \approx 0.4$  (blue), and b)  $\sigma^A(t) \approx 1.1$  (red). Note the rearrangement of Ca-F bonds from zigzag to straight shape when comparing a) and b). See SM for a video of the tilt rearrangement around 18 ps.

On the contrary, strongly anharmonic dynamical effects such as point defect formation in CuI or extended rearrangements in  $\text{KCaF}_3$  involve multiple meta-stable geometries that need to be accounted for. Besides providing a microscopic explanation of the insulating character of these materials, our findings suggest a fundamentally different route for reducing  $\kappa$  that is complementary to traditional phonon-based approaches [43, 44]: For instance, incorporating defects that promote the formation of additional meta-stable states [45, 46] can strengthen the anharmonic effects leading to low thermal conductivity even at temperatures at which these states are not fully accessible. Our results and the more than 10 nanoseconds of available PBEsol-aiMD trajectories can be used to benchmark the various methods available for computing  $\kappa$  in increasingly anharmonic materials. Similarly, this data lends itself to train machine-learning potentials to accelerate  $\kappa$  predictions in the future [47–49] and to develop improved descriptors for  $\kappa$  [10–12]. In this regard, quantitative models that go beyond the qualitative  $\sigma^A$  scaling used in this work to identify anharmonic materials can accelerate materials’ space exploration considerably.

The electronic-structure theory calculations and aiMD trajectories produced in this project are available via the NOMAD repository [50]. Resources for the plots can be found on figshare [51].

This project was supported by the NOMAD Center of Excellence (European Union’s Horizon 2020 research and innovation program, grant agreement No. 951786), the ERC Advanced Grant TEC1p (European Research Council, grant agreement No. 740233), the North-German Supercomputing Alliance (HLRN), BigMax (the

Max Planck Society’s Research Network on Big-Data-Driven Materials-Science). We acknowledge PRACE for awarding us access to JUWELS at GCS@FZJ, Germany. F.K. acknowledges support from the Swedish Research Council (VR) program 2020-04630, and the Swedish e-Science Research Centre (SeRC). T.P. would like to thank the Alexander von Humboldt Foundation for their support through the Alexander von Humboldt Postdoctoral Fellowship Program.

- 
- [1] J. H. Perepezko, *Science* **326**, 1068 (2009).
- [2] D. R. Clarke, M. Oechsner, and N. P. Padture, *MRS Bulletin* **37**, 891 (2012).
- [3] G. J. Snyder and E. S. Toberer, *Nature Materials* **7**, 105 (2008).
- [4] K. Biswas, J. He, I. D. Blum, C.-I. Wu, T. P. Hogan, D. N. Seidman, V. P. Dravid, and M. G. Kanatzidis, *Nature* **489**, 414 (2012-09).
- [5] P. Ferrando-Villalba, S. Chen, A. F. Lopeandía, F. X. Alvarez, M. I. Alonso, M. Garriga, J. Santiso, G. Garcia, A. R. Goñi, D. Donadio, and J. Rodríguez-Viejo, *The Journal of Physical Chemistry C* **124**, 19864 (2020).
- [6] R. Peierls, *Annalen der Physik* **395**, 1055 (1929).
- [7] P.-C. Wei, S. Bhattacharya, J. He, S. Neeleshwar, R. Podila, Y. Y. Chen, and A. M. Rao, *Nature* **539**, E1 (2016-11).
- [8] T. Zhu, R. He, S. Gong, T. Xie, P. Gorai, K. Nielsch, and J. C. Grossman, *Energy & Environmental Science* **14**, 3559 (2021).
- [9] M. W. Gaultois, T. D. Sparks, C. K. H. Borg, R. Seshadri, W. D. Bonificio, and D. R. Clarke, *Chemistry of Materials* **25**, 2911 (2013).
- [10] S. A. Miller, P. Gorai, B. R. Ortiz, A. Goyal, D. Gao, S. A. Barnett, T. O. Mason, G. J. Snyder, Q. Lv, V. Stvanović, and E. S. Toberer, *Chemistry of Materials* **29**, 2494 (2017).
- [11] L. Chen, H. Tran, R. Batra, C. Kim, and R. Ramprasad, *Computational Materials Science* **170**, 109155 (2019).
- [12] T. A. R. Purcell, M. Scheffler, L. M. Ghiringhelli, and C. Carbogno, “Accelerating material-space exploration by mapping materials properties via artificial intelligence: The case of the lattice thermal conductivity,” (2022), 2204.12968.
- [13] D. A. Broido, M. Malorny, G. Birner, N. Mingo, and D. A. Stewart, *Applied Physics Letters* **91**, 231922 (2007).
- [14] N. K. Ravichandran and D. Broido, *Physical Review B* **98**, 085205 (2018).
- [15] M. Simoncelli, N. Marzari, and F. Mauri, *Nature Physics* **15**, 809 (2019), 1901.01964.
- [16] M. Simoncelli, N. Marzari, and F. Mauri, *Physical Review X* **12**, 041011 (2022), 2112.06897.
- [17] U. Aeginolaza, R. Bianco, L. Monacelli, L. Paulatto, M. Calandra, F. Mauri, A. Bergara, and I. Errea, *Physical Review Letters* **122**, 075901 (2019), 1807.07726.
- [18] A. Ioffe and A. Regel, *Prog. Semicond* **4**, 237 (1960).
- [19] A. Marcolongo, P. Umari, and S. Baroni, *Nature Physics* **12**, 80 (2016).
- [20] C. Carbogno, R. Ramprasad, and M. Scheffler, *Physical Review Letters* **118**, 175901 (2017), 1608.06917.
- [21] R. Kubo, *Journal of the Physical Society of Japan* **12**, 570 (1957).
- [22] R. Kubo, M. Yokota, and S. Nakajima, *Journal of the Physical Society of Japan* **12**, 1203 (1957).
- [23] V. Blum, R. Gehrke, F. Hanke, P. Havu, V. Havu, X. Ren, K. Reuter, and M. Scheffler, *Computer Physics Communications* **180**, 2175 (2009).
- [24] F. Knuth, C. Carbogno, V. Atalla, V. Blum, and M. Scheffler, *Computer Physics Communications* **190**, 33 (2015).
- [25] J. P. Perdew, A. Ruzsinszky, G. I. Csonka, O. A. Vydrov, G. E. Scuseria, L. A. Constantin, X. Zhou, and K. Burke, *Physical Review Letters* **100**, 136406 (2008), 0711.0156.
- [26] A. J. C. Ladd, B. Moran, and W. G. Hoover, *Physical Review B* **34**, 5058 (1986).
- [27] F. Knoop, M. Scheffler, and C. Carbogno, arXiv preprint arXiv:2209.01139 (2022).
- [28] F. Knoop, T. Purcell, M. Scheffler, and C. Carbogno, *Journal of Open Source Software* **5**, 2671 (2020).
- [29] F. Knoop, “Heat transport in strongly anharmonic solids from first principles,” (2022).
- [30] F. Knoop, T. A. R. Purcell, M. Scheffler, and C. Carbogno, “Supplemental material,” (2022).
- [31] J. J. Plata, P. Nath, D. Usanmaz, J. Carrete, C. Toher, M. d. Jong, M. Asta, M. Fornari, M. B. Nardelli, and S. Curtarolo, *npj Computational Materials* **3**, 45 (2017).
- [32] Y. Xia, V. I. Hegde, K. Pal, X. Hua, D. Gaines, S. Patel, J. He, M. Aykol, and C. Wolverton, *Physical Review X* **10**, 041029 (2020).
- [33] F. Knoop, T. A. R. Purcell, M. Scheffler, and C. Carbogno, *Physical Review Materials* **4**, 083809 (2020), 2006.14672.
- [34] J. Frenkel, *Zeitschrift für Physik* **35**, 652 (1926).
- [35] D. A. Keen and S. Hull, *Journal of Physics: Condensed Matter* **7**, 5793 (1995).
- [36] Y. Zhu, Y. Liu, M. Wood, N. Z. Koocher, Y. Liu, L. Liu, T. Hu, J. M. Rondinelli, J. Hong, G. J. Snyder, and W. Xu, *Chemistry of Materials* **31**, 8182 (2019).
- [37] J. J. Plata, V. Posligua, A. M. Márquez, J. F. Sanz, and R. Grau-Crespo, *Chemistry of Materials* (2022), 10.1021/acs.chemmater.2c00336.
- [38] H. Xie, Y. Liu, Y. Zhang, S. Hao, Z. Li, M. Cheng, S. Cai, G. J. Snyder, C. Wolverton, C. Uher, V. P. Dravid, and M. G. Kanatzidis, *Journal of the American Chemical Society* **144**, 9113 (2022).
- [39] F. Bertolotti, L. Protesescu, M. V. Kovalenko, S. Yakunin, A. Cervellino, S. J. L. Billinge, M. W. Terban, J. S. Pedersen, N. Masciocchi, and A. Guagliardi, *ACS Nano* **11**, 3819 (2017).
- [40] J. Klarbring, *Physical Review B* **99**, 104105 (2019), 1802.09632.
- [41] A. Bulou, J. Nouet, A. W. Hewat, and F. J. Schäfer, *Ferroelectrics* **25**, 375 (2011).
- [42] T. Tadano and S. Tsuneyuki, *Physical Review Letters* **120**, 105901 (2018), 1710.00311.
- [43] J. Garg, N. Bonini, B. Kozinsky, and N. Marzari, *Physical Review Letters* **106**, 045901 (2011).
- [44] A. J. H. McGaughey, M. I. Hussein, E. S. Landry, M. Kaviani, and G. M. Hulbert, *Physical Review B* **74**, 104304 (2006), cond-mat/0606153.
- [45] C. Carbogno, C. G. Levi, C. G. Van de Walle, and M. Scheffler, *Physical Review B* **90**, 144109 (2014).
- [46] A. Dobrovolsky, A. Merdasa, E. L. Unger, A. Yart-

- sev, and I. G. Scheblykin, *Nature Communications* **8**, 34 (2017).
- [47] G. C. Sosso, D. Donadio, S. Caravati, J. Behler, and M. Bernasconi, *Physical Review B* **86**, 104301 (2012).
- [48] P. Korotaev, I. Novoselov, A. Yanilkin, and A. Shapeev, *Physical Review B* **100**, 144308 (2019).
- [49] C. Verdi, F. Karsai, P. Liu, R. Jinnouchi, and G. Kresse, *npj Computational Materials* **7**, 156 (2021).
- [50] "<https://dx.doi.org/10.17172/nomad/2021.11.11-1>," .
- [51] "<https://dx.doi.org/10.6084/m9.figshare.20310195>," .